GODDARD 428
GRANT
IN-75-CR

Experimental and Theoretical study of Artifical PlasmaLayers Produced by Two Intersecting Beams in a Chamber

NAG5-1051 133339

Technical Report for the work supported by
AFGL throught
NASA Grant No. NAG5-1051

S. P. Kuo
Principal Investigator

Y. S. Zhang

A. Bragg Scattering of EM Waves by Microwave Produced Plasma Layers

This work has been summarized in a paper which is accepted for publication in the Physics of Fluids B and is included in Appendix A.

B. Propagation of High Power Microwave Pulses in Air Breakdown Environment

This work has been summarized in a paper which is submitted for publication in the Journal of Applied Physics and is included in Appendix B.

C. Decay of Plasma Density and Temperature

Three different probes, consisting of an optical probe monitoring the airglow enhancement of the generated plasma, a Bragg scattering probe to detect the temporal evolution of the scattering signal, and a Langmuir double probe to measure the V-I characteristics of the plasma, are used to determine the decay rate of the plasma.

The results show that the initial decay of the plasma is caused by the dissociative attachment loss. The decay time is about 16 μs and electron density is dropped from the initial value $10^{11}cm^{-3}$ to about $3 \times 10^{9}cm^{-3}$ in 70 μs. By this time, the density of negative molecules produced through the electron attachment process has already built up, the electrons generated through detachment process balance the attachment loss. The electron loss rate is then reduced over a factor 10 from the initial decay rate. The temporal evolution of the Bragg scattering test signal has been measured for up to 100 μs to demonstrate the change of loss rate (Fig. 5a of Section IIA.) The Langmuir double probe is then used for plasma measurement for up to 20 ms. It is shown that the plasma density still remains at $10^{7}cm^{-3}$ level after the microwave is off for 10 ms. The results also show that the electron temperature decays much faster than the density as shown in Fig. 1. The maximum electron temperature is about 1 eV.

We next present the ongoing theoretical work.

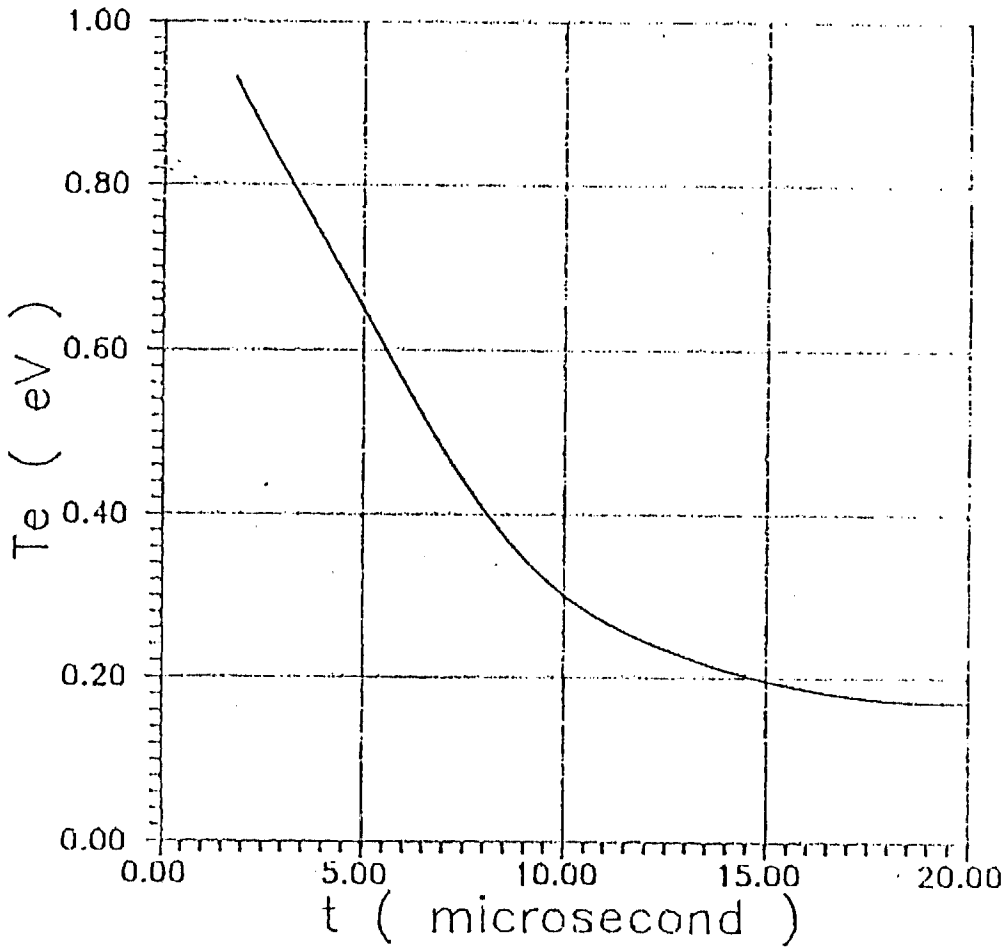

Fig. 1 Electron temperature Vs. time

D. Theoretical Model and Numerical Results of Pulse Propagation in the Air

The plasma is simply described by a rate equation for the electron density as

$$\frac{\partial}{\partial t}n = (\nu_i - \nu_a)n - \nu n^2 \qquad (1)$$

where ν_i, ν_a and γn are the ionization, attachment and recombination rates respectively, for the air, $\nu_i = 0.94\,\nu_s \bar{P}\, e^{6(1-\bar{P}^{-1/2})}[1+1.3\,e^{-3\bar{P}^{-1/2}}]$; $\bar{P}=P/P_c$, P and P_c are power density of the pulse and the threshold power for breakdown at a given gas pressure respectively.

Using the forward scattering approximation, the propagation of the pulse can be described by the Poynting's theorem as shown to be

$$\frac{\partial}{\partial t}P + \frac{\partial}{\partial z}V_g P = -\beta P \qquad (2)$$

where $\beta = \nu\omega_p^2/(\omega^2+\nu^2) \approx \nu\, n/n_c$ and $V_g = c(1-n/n_c)^{1/2}$; P is the power density of the EM wave, n_c is the cutoff electron density of the wave, β is the loss rate of the wave in the plasma through electron-neutral collision. ν is the electron-neutral collision frequency and V_g is the group velocity of the wave.

A new numerical package from the library of the Pittsburgh Supercomputing Center is used to solve Eqs. (1) and (2). Considering first the propagation of pulses in a constant pressure air, the results of numerical calculation for several different initial pulse intensitires are presented in Fig. 1. We are now in the process to compare the numerical results with our experimental results which are intended to be used for improving our theoretical model and determining some physical quantities such as the collision frequency and attachment rate, etc. Once the agreement between numerical and experimental results is reached, a more general case considering the propagation of pulses through the atmosphere will be studied.

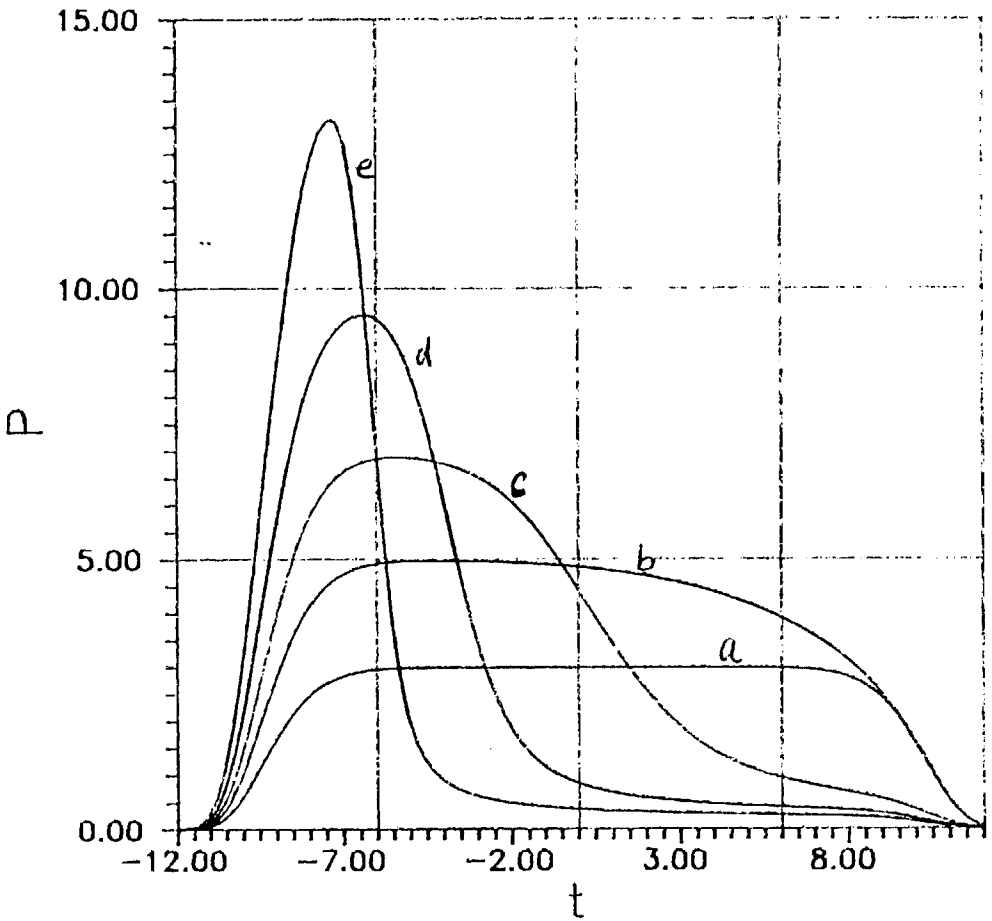

Fig. 1 Transmitted pulse envelopes for five different initial pulse intensities. P_o= a) 3, b) 5, c) 7, d) 10, e) 15. N_o=10E6 cm^{-3}

Appendix A

BRAGG SCATTERING OF EM WAVES BY MICROWAVE PRODUCED PLASMA LAYERS

S.P. Kuo and Y.S. Zhang

Weber Research Institute, Polytechnic University

Route 110, Farmingdale, NY 11735

ABSTRACT

A set of parallel plasma layers is generated by two intersecting microwave pulses in a chamber containing dry air at a pressure comparable to the upper atmosphere. The dependencies of breakdown condition on the pressure and pulse length are examined. The results are shown to be consistent with the appearance of tail erosion of microwave pulse caused by air breakdown. A Bragg scattering experiment by using the plasma layers as Bragg reflector is then performed. Both time domain and frequency domain measurements of wave scattering are conducted. The experimental results are found to agree very well with the theory.

I. INTRODUCTION

Over the years there have been considerable efforts in investigating the propagation of high power microwave pulses through the air. Ionization enhances the electron density in the plasma trail following the pulse and in turn, radically modifies wave propagation[1-6]. However, the possibility of generating plasma layers by high power radio waves in the atmosphere at heights of 30-60 km was first studied theoretically by A. V. Gurevivch and his coworkers[7-10]. An artificial atmospheric plasma is thought to be capable of reflecting radio waves and extends the capability of ionospheric radio communications. In general, there are two processes can be used for the reflection of radio waves. One process is through the cutoff reflection for which the frequency of the incident wave has to be lower than the maximum effective plasma frequency. Therefore, the maximum frequency of radio wave reflecting from the plasma is determined by the electron density of the plasma and the collision frequency between electrons and neutrals. On the other hand, if the plasma is structured with layers, it is believed that Bragg scattering would be an effective process reflecting radio wave off the plasma layers. In this case, there is no upper bound in the frequency of reflection, however, the Bragg condition determines the region of frequency of radio wave for achieving the maximum reflection. One of the apparent advantages of the Bragg scattering process is that much less dense plasma than that required for the cutoff reflection process can be used for reflecting waves of same frequencies. This implies that much less power is needed for plasma generation and its sustainment if the Bragg scattering process is adopted. Although the use of Bragg scattering process requires the scattering plasma to be structured, it may well be the inherent property of the plasma depending on the scheme of plasma generation.

It turns out that the most promising way for plasma generation by electromagnetic radiation is to strike a discharge in the intersection region of parallel polarized wave beams[11]. The interference between the fields of the two beams (for example) enhances the peak field amplitude and, thus, reduces the required power level of each γf beam. This, in turn, helps to reduce the propagation loss in pulse energy before the two beams intersect. In fact, more energy will be delivered to the destination because the pulse tail erosion problem can be almost completely supressed, especially when the intersection altitude is chosen to be near 50 km (1

torr pressure) where the breakdown threshold (for γf pulses in GHz frequency range) is minimum (so that the most effective ionization can be achieved). In the intersection region, field amplitude varies periodically in space in the direction perpendicular to the plane bisecting the two beams. Consequently, the induced ionization patch consists of a set of parallel plasma layers, as an ideal set up for Bragg scattering purpose.

In this paper, we report some laboratory experiments on the characteristic features of air breakdown produced by two microwave beams intersecting at right angle to each other and Bragg scattering of test waves off the induced plasma layers. The organization of this report is as follows. The experimental set-up is described in Sec. II, in which the experimental results characterizing the dynamics and structure of induced plasma are also given. In Sec. III the Bragg scattering experiment is reported. Both time domain and frequency domain measurements of scattering signals are performed. The experimental results are compared with the theory. The work is summarized and discussed in Sect. IV.

II. CHARACTERISTICS OF AIR BREAKDOWN BY MICROWAVE PULSES

Chamber experiments to study the Bragg scattering off microwave-generated plasma layers are conducted. The chamber is a two foot plexiglass cube that is filled with dry air to a pressure corresponding to the simulated altitude. The microwave power is generated by a single magnetron tube (OKH 1448) driven by a soft tube modulator. The magnetron delivers 1 megawatt peak output power at a center frequency of 3.3 GHz. The modulator uses a pulse forming network having a pulse width which can be varied from 1.1 μs to 3.3 μs, with respective repetition rates from 60 to 20 Hz. The microwave beams are fed into the cube, with parallel polarization direction, by two S-band microwave horns placed at right angles to the adjacent sides. The plasma layers are then generated in the central region of the chamber where the two beams intersect. Shown in Fig. 1 is a photo of the plasma layers which are manifested by the enhancement of the airglow from the corresponding locations. A maximum of eight layers can be generated, though only a few of them are shown in the photo. Shown in Fig. 2(a) is the typical envelope of a 1.1 μs pulse used for plasma generation. Using a focusing lens to localize the enhanced airglow, its temporal evaluation between the two consecutive pulses is then recorded on the oscilloscope through a photomultiplier tube. A typical result is shown in Fig. 2(b), which shows the growth and decay of the enhanced ionization. We have also measured the breakdown threshold field as a function of the pressure. The microwave field is measured by a microwave probe which has been calibrated by a known waveguide field. The breakdown threshold is defined as the wave field which is able to enhance minimum observable airglow monitored by the photomultiplier tube. Shown in Fig. 3 are the Paschen breakdown curves for the cases of 1.1 and 3.3 μs pulses. Since a shorter pulse requires a larger ionization rate in order to generate the same amount of electrons (which are proportional to the enhanced airglow flux), the threshold field is, therefore, accordingly increased. This tendency is clearly demonstrated in Fig. 3. It shows that the breakdown threshold field for 1.1 μs pulse is always larger than that for a 3.3 μs pulse. The results also show that in both cases, the breakdown threshold field decreases with a decrease in air pressure and reaches a minimum in the 2 to 1 torr region where $\omega \simeq \nu_c$; ω and ν_c are the microwave frequency and electron-neutral collision frequency, respectively. With a further decrease in the pressure, the breakdown threshold field

increases again. The increase of the threshold field happens also because the wave is in the pulse mode. The ionization frequency and collision frequency are proportional to the neutral density; lower pressure requires a larger field in order to maintain the ionization frequency.

The dependence of the breakdown threshold field on the pressure is also manifested by a similar dependence of the degree of attenuation in the tail portion of a single transmitted pulse through the chamber. The experiment is performed by reducing the chamber pressure consecutively from 8 torr to 50 m torr, while the incident pulse is fixed at constant amplitude. A series of snap shots demonstrating this behavior is presented in Fig. 4. In the high pressure region ($\geq$ 8 torr), the breakdown threshold field is higher than that of the incident pulse, and therefore, very little ionization can occur; thus, the pulse can pass through the chamber almost without any distortion (Fig. 4(a)). However, as the pressure drops, the breakdown threshold also decreases before reaching the minimum, and hence, more ionization occurs and so does more distortion to the pulse (Figs. 4(b)-4(d)). The distortion always starts from the tail portion of the pulse (i.e. tail erosion) because it takes finite time for the plasma to build up and thus, maximum absorption of pulse energy by the generated electrons always appears in the tail of the pulse. Consequently, the leading edge of the pulse is usually not affected. Between 2 to 1 torr, the pulse appears to suffer maximum tail erosion and hence only the very narrow leading edge of the pulse can pass through the chamber (Figs. 4(e) and 4(f)). The tail erosion becomes weak again for a further decrease in the pressure (Figs. 4(g)-4(j)) and eventually vanishes (Fig. 4(k)) once the pressure becomes so low ($\leq$ 0.05 torr) that the breakdown threshold power exceeds the peak power of the incident pulse.

III. BRAGG SCATTERING

The plasma layers generated by the two crossed microwave pulses are used for the Bragg scattering study. The spatial distribution of the plasma layers is first measured with a Langmuir double probe. This is done by using a microwave phase shifter to move the plasma layers across the probe. The peak density distribution for a spatial period is thus obtained and presented in Fig. 5. The result shows that we have indeed produced very sharp plasma layers with very good spatial periodicity (Fig. 1). A Bragg scattering experiment has then been conducted and described as follows.

Presented in Fig. 6 is a block diagram of the experiment setup. In addition to the facility used for plasma generation (located to the left of the plexiglass chamber), a sweep microwave generator (4-8 GHz) is used to generate a test wave which is incident into the chamber through a C-band horn. The incident angle of the test wave with respect to the normal of the plasma layers is 45 degrees. Hence, the S-band horn #2 located at a right angle to the adjacent side can be used as the receiver of the Bragg scattering test wave. In order to separate the Bragg coherent reflection mechanism from the cutoff reflection mechanism, the test wave is swept in a frequency range much higher than the plasma cutoff frequency. Consequently, the test wave will be received by the S-band horn #1 even while the plasma is present. The amplitude of this undesired signal is reduced by using a directional coupler; nevertheless, it represents a large noise to the real scattering signal. To resolve this problem, a standard noise cancellation technique is used. The microwave components used for noise cancellation are shown in the diagram (Fig. 6). An HP spectrum analyzer (8569B) is used for recording the scattering signal. It is noted that the attenuation of the directional coupler is frequency dependent. Only test waves with frequencies leading to more than 15 db attenuation of the directional coupler are used in the experiment. Consequently, the perturbations of the noise signal due to the presence of the plasma, which in principle is in the same intensity level as the scattering signal, is reduced by 15 or more db and will not affect the measurement of the Bragg scattering signal.

Presented in Fig. 7 are the outputs of the spectrum analyzers for two cases. Fig. 7(a) shows that no signal is received when there is no plasma. However, an appreciable scattering

signal is detected, as shown in Fig. 7(b) whenever the plasma layers are produced. The frequency of the test wave is 4.01 GHz, which is much higher than the cutoff frequency. A clear signature of Bragg scattering has been demonstrated. The temporal evaluation of the scattering signal has also been measured. The result for a test wave with frequency 5.5 GHz is presented in Fig. 8(a). For comparison, one of the two microwave pulses (both are 1.1 μs) used for plasma generation is shown in Fig. 8(b). As one can see, the scattering signal continues to persist for about 100 μs after the breakdown pulses are turned off. This result indicates that the coherent scattering process can be very effective even when the plasma frequency is well below (~2 order of magnitude) the cutoff frequency of the test wave.

The next question is how the experimental results compare with the theory. Considering a set of N parallel plasma slabs with thickness δ and separation d, and using the Bragg condition $2d \sin\theta = n\lambda_s$, where θ is the angle of Bragg scattering, λ_s is the wavelength of the scattered wave, and n is a positive integer, the scattering (reflection) coefficient S of wave intensity is derived analytically and expressed as

$$S = |\varepsilon_r/\varepsilon_t|^2 = (k_t^2\alpha/2)^2 [\sin(n\pi\delta/d) / (n\pi/d)^2]^2 [\sin N\theta_t/\sin\theta_t]^2 , \quad (1)$$

where ε_t and ε_r are the field amplitudes of test wave and scattering Wave, respectively; $\alpha = \omega_{pe}^2/\omega_t(\omega_t^2+\nu_c^2)^{1/2}$; k_t and ω_t are the wave number and frequency of the test wave; and $\theta_t = (\omega_t-\omega_s)d\sin\theta/c$ and $\omega_s = 2\pi c/\lambda_s$.

This reflection coefficient is then plotted as a function of the test wave frequency in Fig. 9. By sweeping the test wave frequency, such a dependence is also determined experimentally in a relatively small frequency range (4.3 GHz to 7.8 GHz) and presented in Fig. 9 for comparison. The frequency dependencies of output intensity of the sweep generator and the antenna gain of the receiving horn (S-band horn #2) have been examined and taken into account in calibrating the intensity of the scattering signals. Though a maximum eight layers can be produced, only three of them have significant overlap along a line of sight. Therefore, only these layers can significantly contribute to the Bragg scattering process. Besides an uncalibrated absolute magnitude, the two functional dependencies are shown to agree with each other very well. It is noted that the separation d between the two adjacent plasma layers is related to the wavelength

λ_o of the microwave pulses and the angle ϕ between the propagation directions of the two intersecting pulses with the relationship $d = \lambda_o/2 \sin(\phi/2)$. Using the Bragg condition $2d \sin\theta = n\lambda_s$, the optimum frequency for Bragg scattering is given by

$$f_s = nf_o \sin(\phi/2)/\sin\theta \, .$$

In the present experiment, $\phi = 90°$ and $\theta = 45°$, and thus $f_s = nf_o$. This indicates that the frequency of the test wave, which satisfies the Bragg condition for the current experimental arrangement, is equal to the frequency and its harmonics of the breakdown pulses. Consequently, the breakdown wave can not be filtered out and represents a very strong noise, which prevents any meaningful test of Bragg scattering at these frequencies, and in fact, also in the neighborhood frequency regions. Although the optimum frequency region for Bragg scattering is not examined, nevertheless the consistency between prediction and experimental results may lead us to conclude, based on the maximum theoretical reflection coefficient, that plasma layers can indeed be an effective Bragg reflector, especially if more layers can be produced for scattering purposes.

IV. SUMMARY AND DISCUSSION

Plasma layers generated by two intersecting microwave pulses are used for the study of Bragg scattering. The experiment is conducted in a large plexiglass chamber shielded with a microwave absorber so that the microwave reflection from the wall can be minimized. Hence, the experiment can be considered to be a laboratory simulation of conceptualized plasma layers generated by high power radio waves in the upper atmosphere, as investigated theoretically by Gurevich.

We first determine the characteristics of air breakdown by powerful microwave pulses. We have observed that it is very difficult to generate plasma in the center of the chamber with a single pulse. This is mainly because the plasma generated near the wall adjacent to the microwave horn causes erosion of the tail of the incident pulse and the pulse becomes too short, by the time it reaches the central region of the chamber, to cause appreciable ionization. However, this problem is easily overcome when the scheme of two intersecting pulses is used for plasma generation. In this approach, each pulse has its field amplitude below the breakdown threshold to avoid the tail erosion. However, the fields in the intersecting region can add up and exceed the breakdown threshold. This scheme is most effective when the two pulses have the same polarization and are coherent. In this case, the wave fields form a standing wave pattern in the intersecting region in the direction perpendicular to the bisecting line of the angle ϕ between the intersecting pulses. Thus, parallel plasma layers with a separation $d = \lambda_o/2 \sin(\phi/2)$ can be generated. This result is shown in Fig. 1.

Since there are no electrodes involved in the current experiment of air breakdown, we can determine the breakdown threshold field as a function of the air pressure within the accuracy of microwave probe measurement. Two Paschen breakdown curves for the cases of 1.1 and 3.3 μs pulses are determined as shown in Fig. 3. The appearance of a Paschen minimum can be explained as the result of breakdown by a short pulse which is equivalent to a dc discharge with short separation between electrodes (i.e., short electron transit time). The result that the breakdown threshold by a longer pulse (3.3 μs) is lower than that by shorter pulse (1.1 μs) agrees with the explanation The characteristic of the curves is also confirmed

phenomenologically by the various degrees of tail erosion of the same pulse passing through the chamber at different pressures, as shown in Fig. 4.

An optical probe has been used to monitor the growth and decay of airglow enhanced by microwave generated electrons. Two processes are, in general, responsible for the airglow. One is through the electron-ion recombination and the other one is through impact excitation of natural gas. Since only weakly ionized plasma is generated, the second process is believed to be dominant. However, the second process requires that the electron energy exceed 2*e*V. Therefore, the decay rate of airglow intensity shown in Fig. 2(b) accounts for not only the decay of the electron density caused by the dissociative attachment loss but also for the decay of the electron temperature caused by energy loss to the neutrals and the loss of fast electrons.

We then conducted the Bragg scattering experiment with the produced plasma layers. Both temporal evaluation of the scattering signal from a test wave and the spectral dependence of the scattering coefficient have been examined. Good agreement between theoretical and experimental results on the spectral dependence of the scattering coefficient has been achieved (Fig. 9). The theoretical result (1) shows that the scattering coefficient is proportional to the square of the electron density and insensitive to the electron temperature. Therefore, the electron decay rate after the breakdown pulses have passed through can be evaluated from Fig. 8(a). It shows that the initial decay rate is about 6×10^4 sec^{-1}, which is consistent with the dissociative attachment rate. It also shows that the electron density after 70 μs is reduced by a factor of about 30. Similarly, the electron decay rate is also reduced over a factor of 10 from the initial decay rate. In this region the decay rate is consistent with the recombination loss rate. This is realized by the fact that when enough negative molecule ions are produced through the electron attachment process, the detachment rate for electron regeneration is increased and eventually balances out the electron attachment loss rate. Thus, the dominant electron loss mechanism is shifted to the recombination process. It should be noted that the attachment process causes only the decay of free electrons. The ion density decays at a relatively slow rate determined by the recombination process and the ambipolar diffusion process.

ACKNOWLEDGEMENT:

We wish to acknowledge useful discussions with Prof. N. Marcuvitz of Polytechnic Univ., with Dr. Paul Kossey of the Air Force Geophysics Laboratory and with Dr. M. C. Lee of Massachusetts Institute of Technology and helpful technical assistance from K. K. Tiong.

This work was supported by the Air Force Geophysics Laboratory through a NASA Grant No. NAG5-1051 and by the Air Force Office of Scientific Research, Air Force Systems Command, Grant No. AFOSR-85-0316.

REFERENCES

1. A. D. MacDonald, D. U. Gaskell, and H. N. Gitterman, Phys. Rev., 5, 1841 (1963).

2. W. M. Bollen, C. L. Yee, A. W. Ali, M. J. Nagurney, and M. E. Read, J. Appl. Phys., 54, 101 (1983); C. L. Yee, A. W. Ali, and W. M. Bollen, J. Appl. Phys., 54, 1278 (1983).

3. J. H. Yee, R. A. Alvarez, D. J. Mayhall, N. K. Madsen, and H. S. Cabayan, J. Radiation Effects Res. and Eng., 3, 152 (1984).

4. B. Goldstein and C. Longmire, J. Radiation Effects Res. and Eng., 3, 1626 (1984).

5. Wee Woo and J. S. DeGroot, Phys. Fluids, 27, 475 (1984).

6. J. H. Yee, R. A. Alverez, D. J. Mayhall, D. P. Byrne, and J. DeGroot, Phys. Fluids, 29, 1238 (1986).

7. A. V. Gurevich, Geomag. Aeronom. 12, 631 (1972).

8. A. V. Gurevich, Geomag. Aeronom. 19, 428 (1979).

9. N. D. Borisov and A. V. Gurevich, Geomag. Aeronom. 20, 841 (1980).

10. A. V. Gurevich, Sov. Phys. Usp. 23, 862 (1981).

11. A. L. Vikharev, V. B. Gil'denburg, O. A. Ivanov, and A. N. Stepanov, Sov. J. Plasma Phys. 10, 96 (1984); A. L. Vikharev, O. A. Ivanov, and A. N. Stepanov, Sov. J. Plasma Phys., 10, 460 (1985).

Fig. 1 Top view of plasma layers produced in the chamber.

Fig. 2 The optical measurement of the growth and decay of the airglow from a plasma generated by two intrsecting 1.1 μs microwave pulses.
(a) Envelope of a 1.1 μs microwave pulse; the horizontal axis is 200 ns/division.
(b) Growth and decay of plasma glow measured by an optical probe, 1 μs/division.

Fig. 3 Dependence of the air breakdown threshold field on the pressure for two pulse lengths.

Fig. 4 Pulse received after passing through the chamber at different air pressures.

Fig. 5 Probe measurement of the plasma density distribution along the direction transverse to the plasma layers. Measurement is from the central point x=0 of one layer to the midpoint x=3.24 of the next layer. The minimum density 10^2 is an estimated value.

Fig. 6 Microwave Bragg scattering experimental set-up.

Fig. 7 Spectrum analyzer CRT display.
(a) No signal is received when the plasma is off.
(b) The spectrum of scattering signals when plasma layers are present.

Fig. 8 The time domain measurement of the scattering signal and the microwave pulse used for plasma generation, 10 μs/division.
(a) Growth and decay of the scattering signal over a 100 μs time interval.
(b) A 1.1 μs pulse similar to that of Fig. 2(a).

Fig. 9 The dependence of the reflectivity S of plasma layers on wave frequency. Experimental and theoretical results. The 0 dB on the vertical axis is an arbitrary reference.

Fig. 1 Top view of plasma layers produced in the chamber

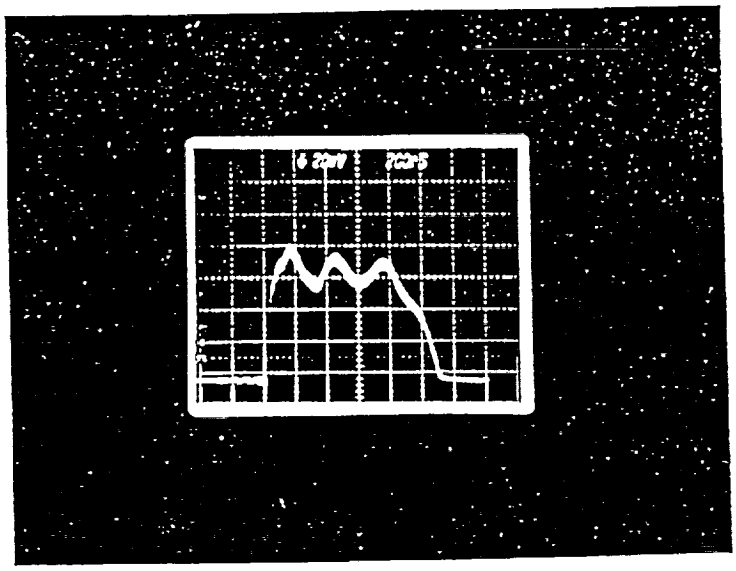

(a) Envelope of a 1.1 μs microwave pulse, horizontal axis is 200 ns/ division.

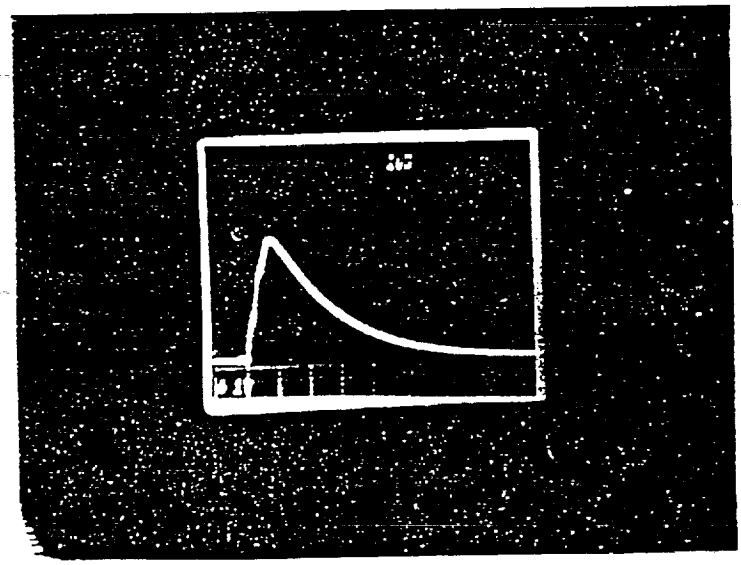

(b) Growth and decay of plasma glow measured by an optical probe, 1 μs/ division

Fig. 2

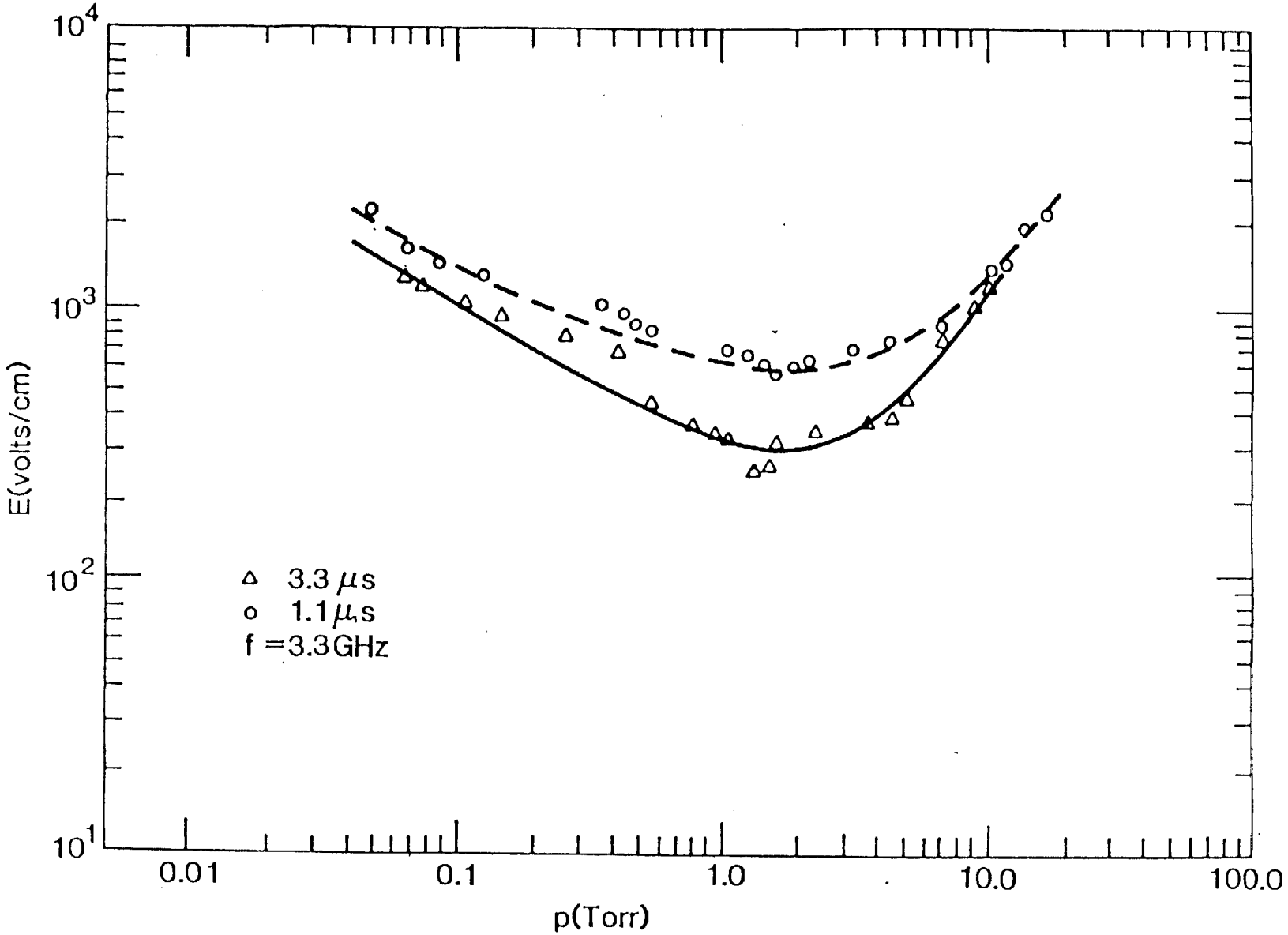

Fig. 3 Dependence of air breakdown threshold field on the pressure for two pulse lengths.

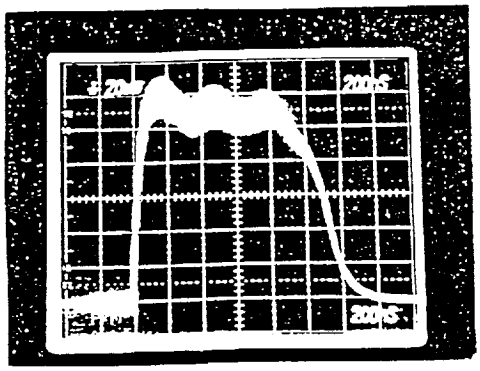

(a) P= 8 torr

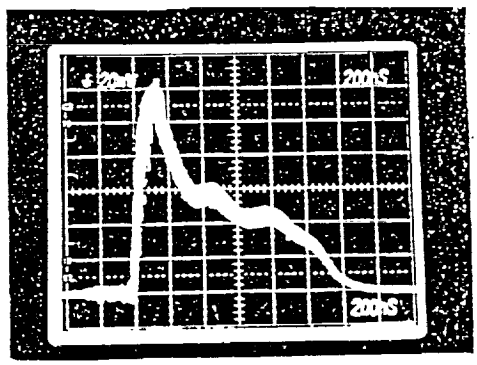

(d) P= 4 torr

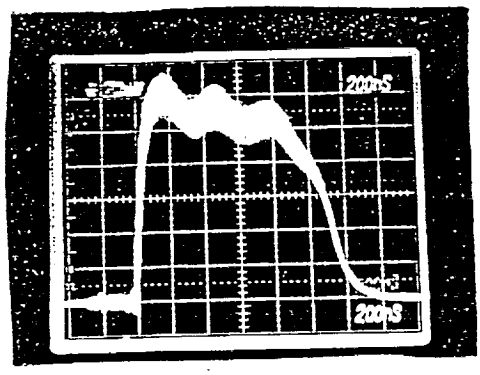

(b) P = 6 torr

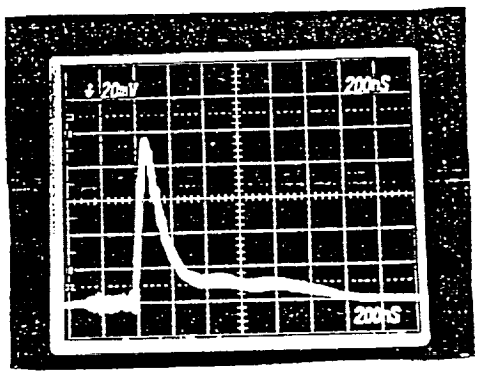

(e) P = 2 torr

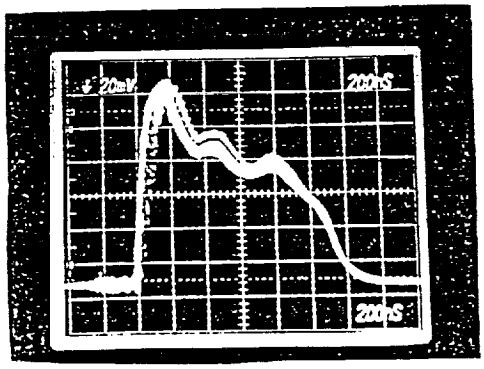

(c) P = 5 torr

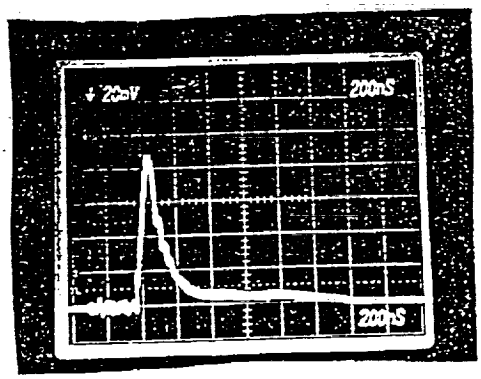

(f) P = 1 torr

Fig. 4 (a - f)

ORIGINAL PAGE
BLACK AND WHITE PHOTOGRAPH

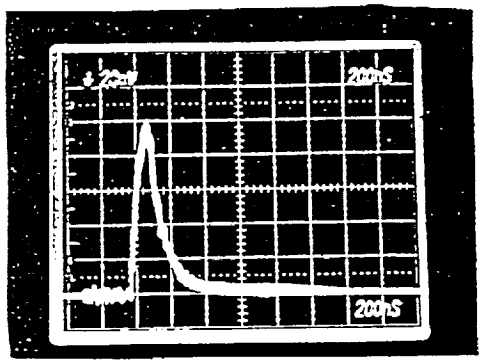

(g) P= 0.45 torr

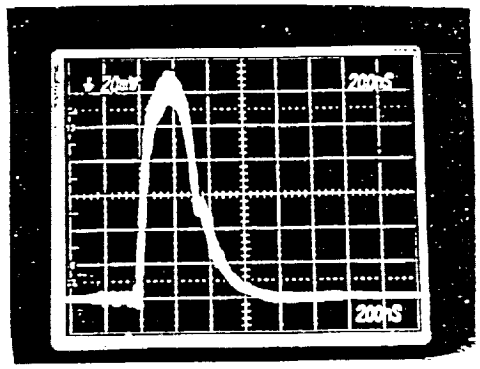

(j) P= 0.07 torr

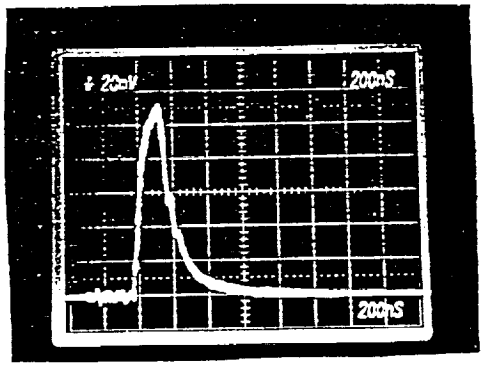

(h) P = 0.2 torr

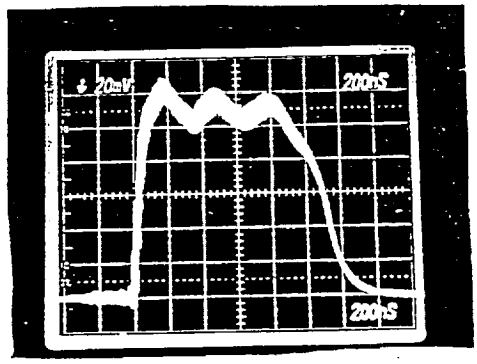

(k) P = 0.05 torr

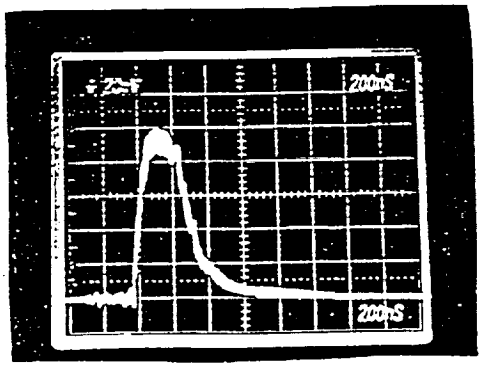

(i) P = 0.1 torr

Fig. 4 (g - k).
Pulse received after passing through the chamber at different air pressures.

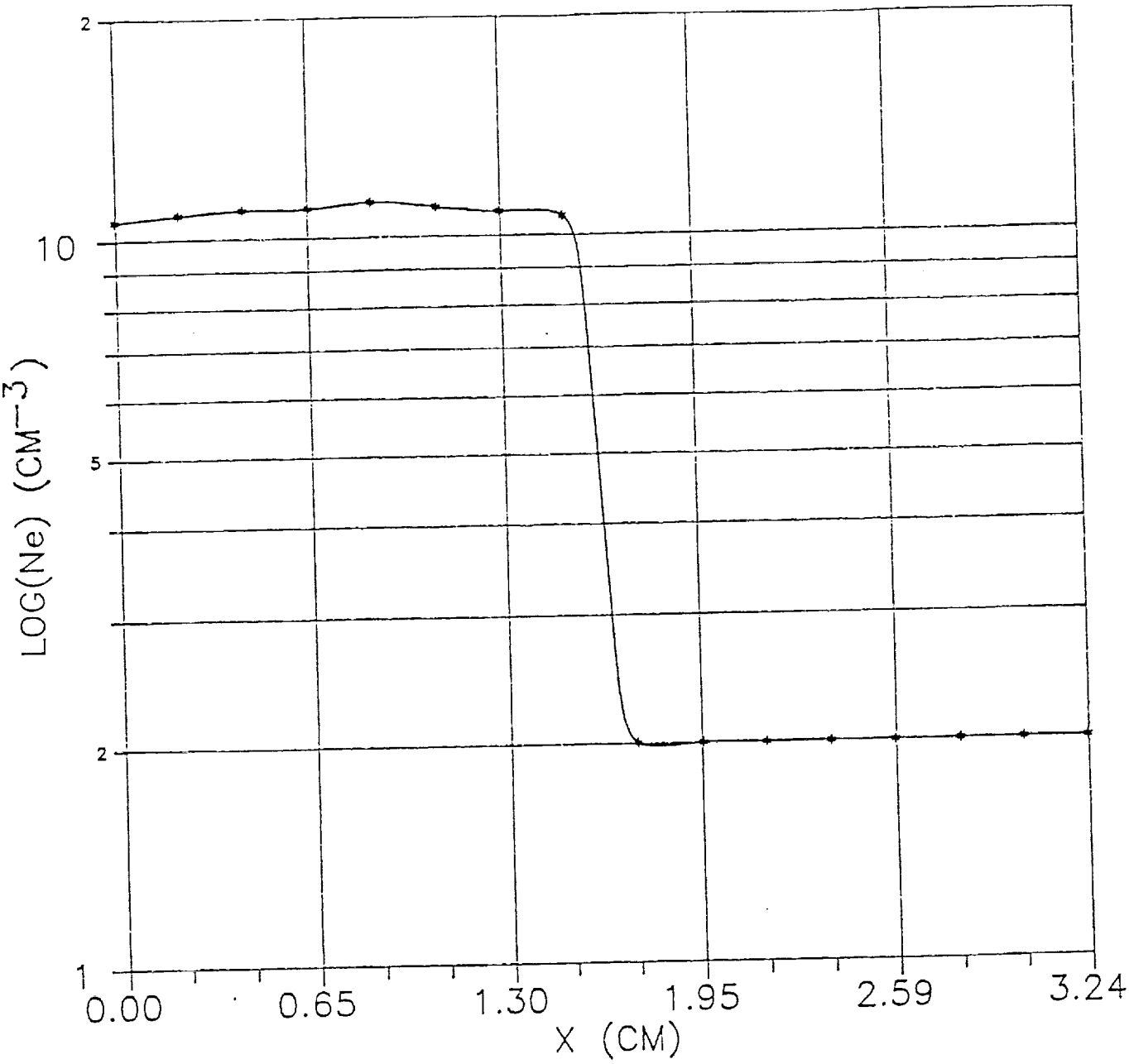

Fig. 5 Probe measurement of the plasma density distribution along the direction transverse to the plasma layers. Measurement is from the central point x=0 of one layer to the midpoint x=3.24 to the next layer. The minimum density 10^2 is an estimated value.

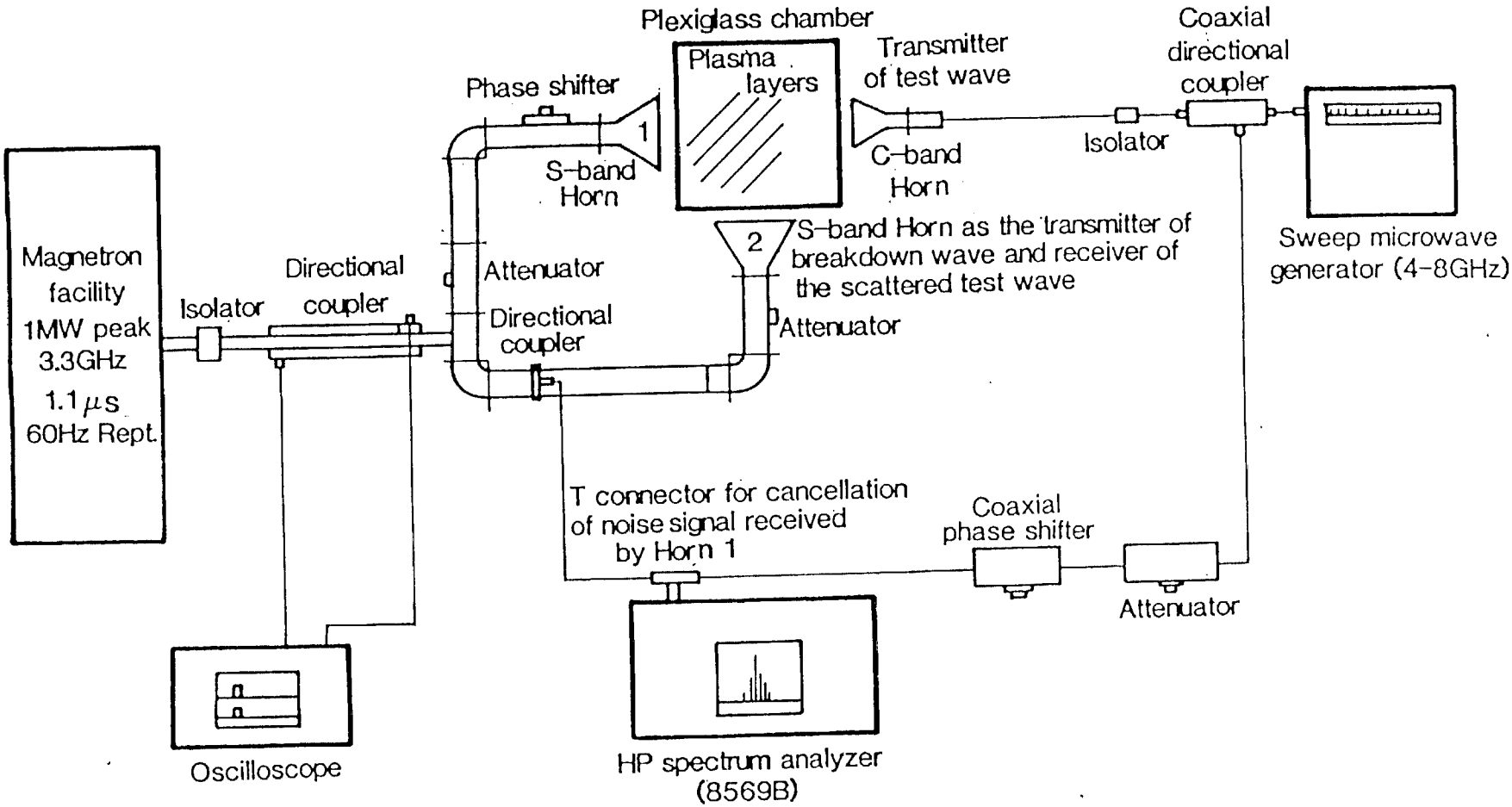

Figure 6 Microwave Bragg scattering experimental set-up

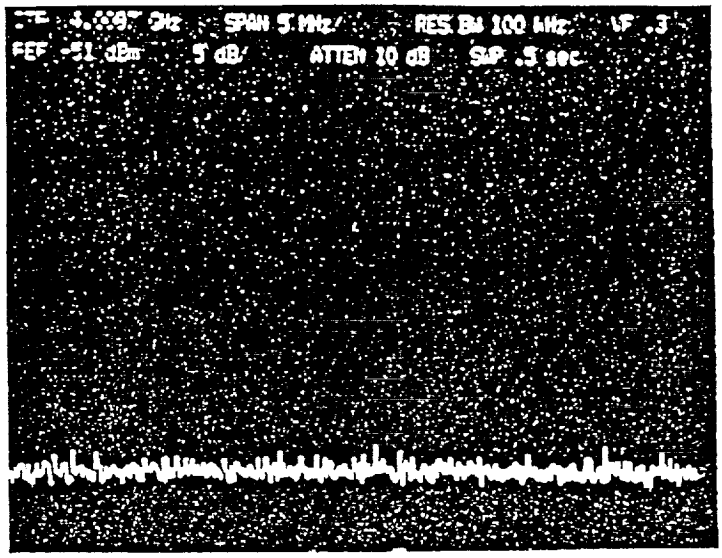

(a) No signal is received when plasma is off.

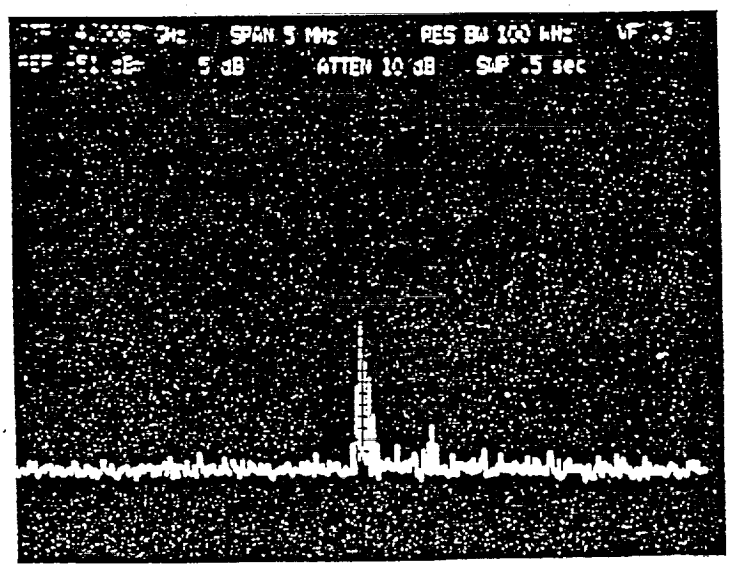

(b) Spectrum of scattering signal when plasma layers are present.

Fig. 7 Spectrum analyzer CRT display.

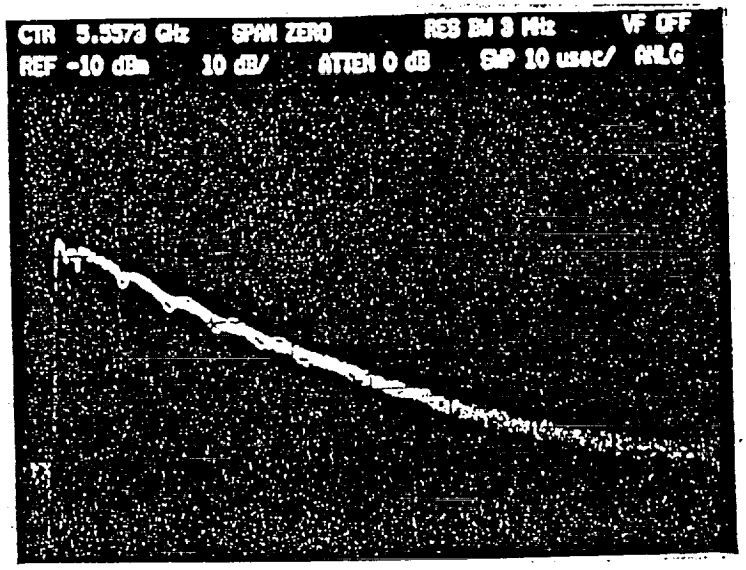

(a) Growth and decay of scattering signal over 100 μs time domain.

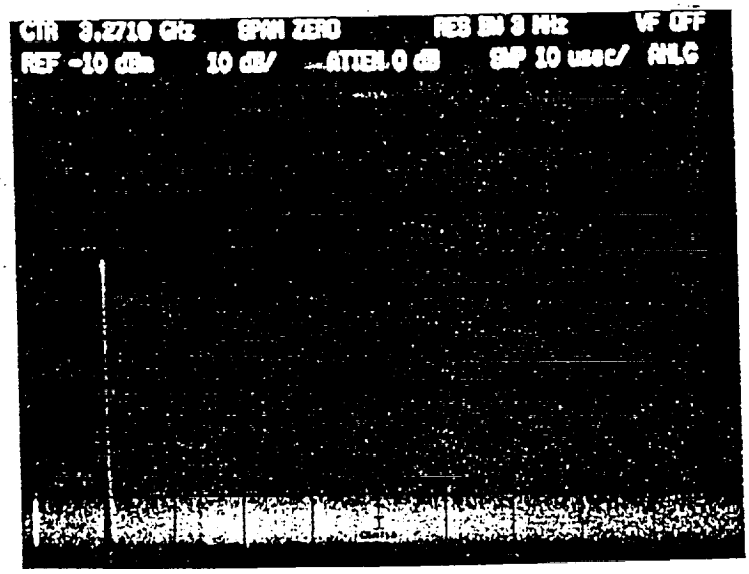

(b) 1.1 μs pulse similar to that of Fig. 2a.

Fig. 8 Time domain measurement of the scattering signal and the microwave pulse used for plasma generation.

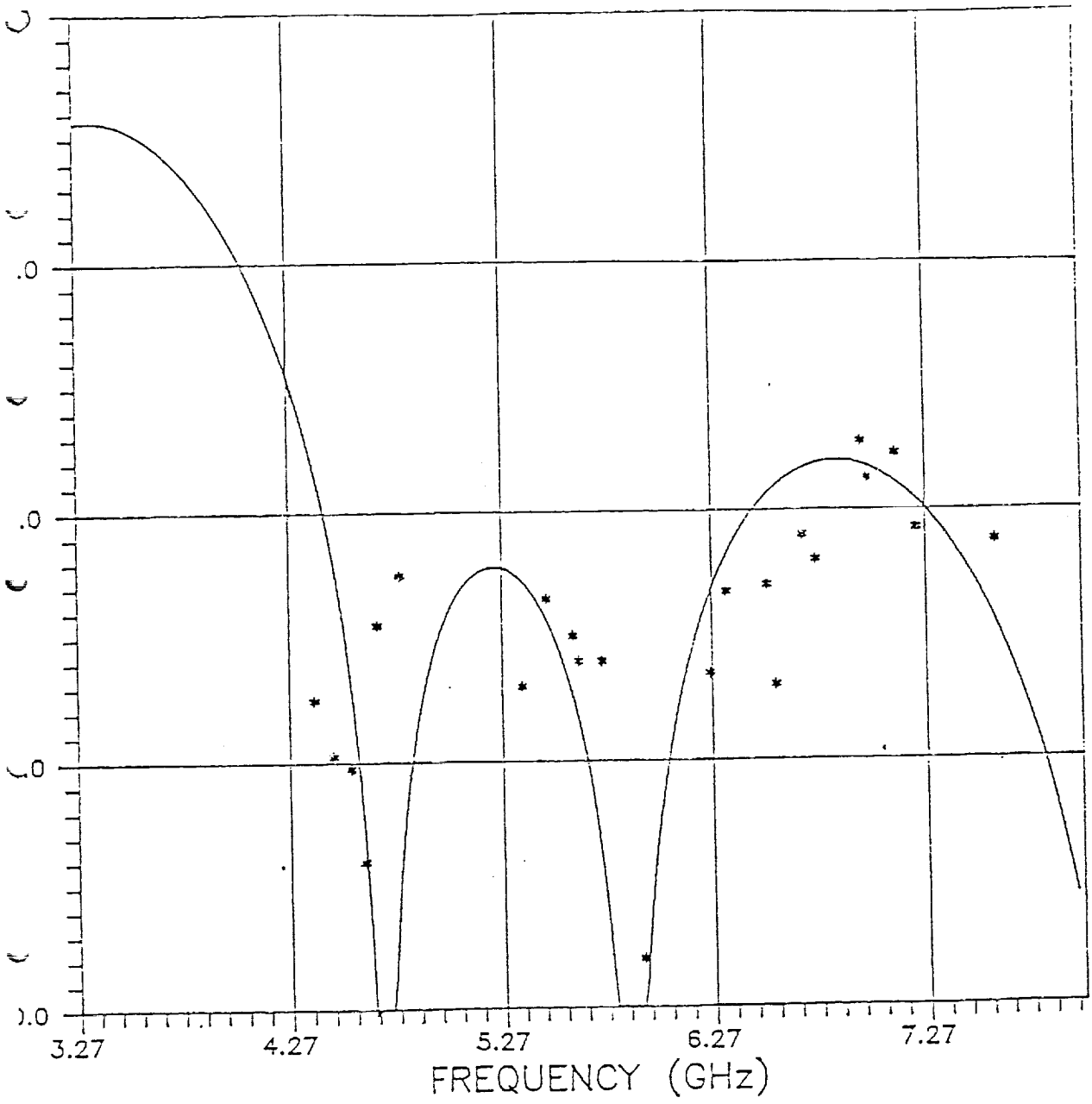
.0
.0
.0
).0
3.27
4.27
5.27
6.27
7.27
FREQUENCY (GHz)

Appendix B

PROPAGATION OF HIGH POWER MICROWAVE PULSES

IN AIR BREAKDOWN ENVIRONMENT

S. P. Kuo and Y. S. Zhang

Department of Electrical Engineering & Computer Science

Polytechnic University,Route 110, Farmingdale, NY 11735,U.S.A.

Paul Kossey

Air Force Geophysics Laboratory, Hanscon AFB, MA 01731,U.S.A.

Abstract

A chamber experiment is conducted to study the propagation of high power microwave pulses through the the air. Two mechanisms responsible for two different degree of tail erosion have been identified experimentally. The optimum pulse amplitude for maximum energy transfer through the air have also been determined.

I. Introduction

The propagation of high power microwave pulses through the atmosphere has been a subject with considerable scientific interest.[1-5] This is because air breakdown produces ionization phenomena that can radically modify wave propagation. Ionization gives rise to a space-time dependent plasma which attenuates the tail of the pulse but hardly affects the leading edge because of the finite time for the plasma to build up. A mechanism which is called "tail erosion" plays the primary role in limiting transmission of pulse.[1-3] Moreover, the nonlinear and non-local effects brought about by the space-time dependent plasma also play important roles in determining the propagation characteristic of the pulses.[5] Therefore, any meaningful theoretical effort requires a self-consistent description of the propagation process. Consequently, an experimental effort could be more relevant and useful.

Basically, there are two fundamental issues to be addressed. One concerns the optimum pulse characteristics for maximum energy transfer through the atmosphere by the pulse. The second concern is maximizing the ionizations in the plasma trail following the pulse. In general, these two concerns are interrelated and must be considered together. This is because in order to minimize the energy loss in the pulse before reaching the destination, one has to prevent the occurrence of excessive ionization in the background air. Otherwise, the overdense plasma can cutoff the propagation of the remaining part of the pulse and cause the tail of the pulse to be eroded via the reflection process. This process is believed to be far more severe in causing tail erosion than the normal process attributed to ionization and heating. Once this process occurs, the remaining pulse will become too narrow to ionize dense enough plasma whose nonlinear effect is thought to be able to help in sufficient focusing to compensate for wave spreading beyond the Fresnel distance.

The purpose of our experimental effort is to understand the fundamental behavior of tail erosion and address the question of how energy loss depends on basic parameters such as pulse intensity and width, and background pressure. The experimental data can then be incorporated for the development of an useful theoretical model for a self-consistent derivation of pulse propagation..

II. Tail erosion mechanisms

Experiments has been conducted in a large chamber made of 2 feet cube of plexiglass and filled with dry air at various pressure. Microwave pulse is fed into the cube by a S-band microwave horn placed at one side of the chamber. A second S-band horn placed at the opposite side of the chamber is used to receive the transmitted pulse. the microwave power is generated by a single magnetron tube (OKH 1448) driven by a soft tube modulator. The magnetron produces 1MW peak output power at a frequency of 3.27 GHz. The modulator uses a pulse forming network (PFN) having a pulse width of 1.1μs and a repetition rate of 60 Hz. The PFN can also be adjusted to increase the pulse width to 3.3μs, while reducing the repetition rate to 20 Hz. Shown in Figure 1 is the block diagram of the experimental setup.

Breakdown of air was detected either visually, as the first sign of a glow in the chamber, or as the distortion in the shape of the pulse received by the horn placed at the opposite side of the chamber. The dependence of the breakdown threshold field on the pressure can thus be manifested by a dependence of the degree of distortion of the tail portion of the transmitted pulse through the chamber. A series of snap shots demonstrating this behavior is presented in Figure 2. In the high pressure regions pictured, the breakdown threshold is expected to be high, therefore, very little ionization can occur and, thus the pulse can pass through the chamber almost without any loss (or distortion). However, as the pressure drops, the breakdown threshold also decreases before reaching the minimum, hence, more ionization occurs and also more distortion to the pulse. The distortion always starts from the tail of the pulse (i.e. tail erosion) because it takes finite time for plasma to build up and thus, maximum absorption of pulse energy by the generated electrons always appears in the tail of the pulse. Consequently, the leading edge of the pulse is usually not affected. Between 1 and 2 torr , the pulse appears to suffer maximum tail erosion and hence only very narrow leading edge can pass through chamber. The tail erosion becomes weak again for a further decrease in the pressure and can eventually be prevented once the pressure becomes so low that the breakdown threshold power exceeds the peak power of the incident pulse.

Tail erosion is a common phenomenon appearing in the propagation of high power microwave pulse (HMP). This phenomenon is further demonstrated by the snap shots presented in Figure 3, where 1.1μs pulses, with four consecutively increasing amplitude, are transmitted into the chamber of

1 torr pressure from one side and received from the opposite side. The first pulse has amplitude below the breakdown threshold, and hence, nothing is expected to happen. Consequently, the received pulse shape is undistorted from that of transmitted pulse. Once the amplitude exceeds the breakdown threshold, more tail erosion occurred to the larger amplitude pulses,as is observed by the subsequent three snap shots.This is because the increase of the ionization rate with field amplitude allows more electrons, which attenuate the pulse, to build up. Now let's focus on the last two pictures. Pulses have been eroded strongly in both cases. However, a clear distinction between the two cases is noticed. In one case corresponding to the third picture, the erosion to the tail of the pulse is not complete. In other words, the received pulse width extends to the original width. In the other case, a large portion of the pulse is more or less eroded completely during the finite propagation period. Obviously it is a different mechanism responsible for the second case. The ionization frequency becomes so large in the second case that the electron density exceeds the cutoff density of the wave before the whole pulse passes through. The overdense plasma screen reflects the remaining portion of the pulse and causes even more severe tail erosion. In summary, two mechanisms responsible for the tail erosion are identified. One is due to attenuation by the self-generated underdense plasma. The other one is caused through reflection by the self-generated overdense plasma screen. These two processes are also verified by the reflected power level measured for each cases. As shown in Figure 4, the snap shots presented on the RHS of the Figure are reflected pulse shape corresponding to each received pulse on its left. As shown by the last set of picture, strong reflection and complete erosion are observed consistently.

In order to avoid cut off reflection, the power of the pulse should be lower than a critical power Pr which is defined as the minimum required power for generating an overdense plasma screen. When overdense plasma screen is formed the shape of the reflected pulse changes drastically and can be monitored easily. Thus, the critical power Pr can be determined. This critical power varies in general with the pressure and pulse width. Measurements are made to determine these functional dependencies as shown in Figure 5, where P=Pr/Pc is the critical power normalized to the breakdown threshold power Pc which has been presented in elsewhere[6]. It is limited by the available microwave power, only region of 0.2 to 10 torr is examined. Nevertheless, this is the region of main concern because air breakdown has the lowest threshold.

IV. Discussion

Our study indicates that an increase of pulse amplitude may not help to increase the energy transfer by the pulse. This is because two tail erosion mechanisms are in play to degrade the energy transfer. A demonstration is presented in Figure 8, where the growth and decay of airglow enhanced by electrons through air breakdown by 3.3μs pulse are recorded for two different power levels. In Figure 8a the power level is below the critical power and the airglow grows for the entire 3.3μs period of the initial pulse width. As power is increased beyond the critical value, the initial growth of the airglow becomes faster as shown in Figure 8b. However, it is also shown in Figure 8b that the airglow saturates at about the same level as that of Figure 8a. Moreover, the airglow already starts to decay even before the 3.3μs period. In other words, cutoff reflection happening in the second case limits the energy transfer by the pulse, the additional energy added to the pulse is wasted by reflection. The way to solve the problem is either to lower the amplitude of the pulse or to narrow the pulse width so that the propagation loss can be minimized. The remaining question is about the optimum parameters for the pulse in order to achieve effective ionization for self-focusing purpose. Unfortunately, this question can not easily be answered by the chamber experiments. This is because the effect of pressure gradient and large propagation distance can not be incorporated in the investigation. Nevertheless, the understanding of the fundamental behavior of tail erosion and the set of obtained experimental data should be very useful for guiding the development of a practical theoretical model.

Acknowledgment

This work is being supported by the Air Force Geophysical Laboratory through NASA Grant No. NAG 5-1051 and by the Air Force Office of Scientific Research Grant No. AFOSR-85-0316. Useful discussion with Dr. M.C. Lee is appreciated.

REFERENCES

1. W.M.Bollen, C. L.Yee, A.W. Ali, M. J. Nagurney, and M. E.Read, J. Appl. Phys. 54, 101 (1983); C. L. Yee, A. W. Ali, and W. M. Bollen, J. Appl. Phys., 54, 1278 (1983).

2. J. H. Yee, R. A. Alvarez, D. J. Mayhall, N. K. Madsen, and H. S. Cabayan, J. Radiation Effects Res. and Eng., 3, 152 (1984).

3. B. Goldstein and C. Longmire, J. Radiation Effects Res. and Eng., 3, 1626 (1984).

4. Wee Woo and J. S. DeGroot, Phys. Fluids, 27, 475 (1984).

5. J. H. Yee, R. A. Alverez, D. J. Mayhall, D. P. Byrne, and J. DeGroot, Phys. Fluids, 29, 1238 (1986).

6. S.P. Kuo and Y.S. Zhang, Phys. Fluids B, submitted.

Figure Captions:

Fig. 1 Experimental setup

Fig. 2 Pulse transmission through chamber at different air pressure

Fig. 3 Tail erosion of microwave pulses

Fig. 4 Transmitted pulses and the corresponding reflected pulses

Fig. 5 The dependence of the normalized critical power P=Pr/Pc
on pressure for two different pulse lengths.

Fig. 6 The growth and decay of enhanced airglow (upper trace). 3.3μs pulses
at two different power levels P1 (for 6a) and P2 (for 6b) are used for causing air breakdown, where p2/p1=1.32. The lower trace of each photo represents the time dependence of the amplitude of the microwave pulse

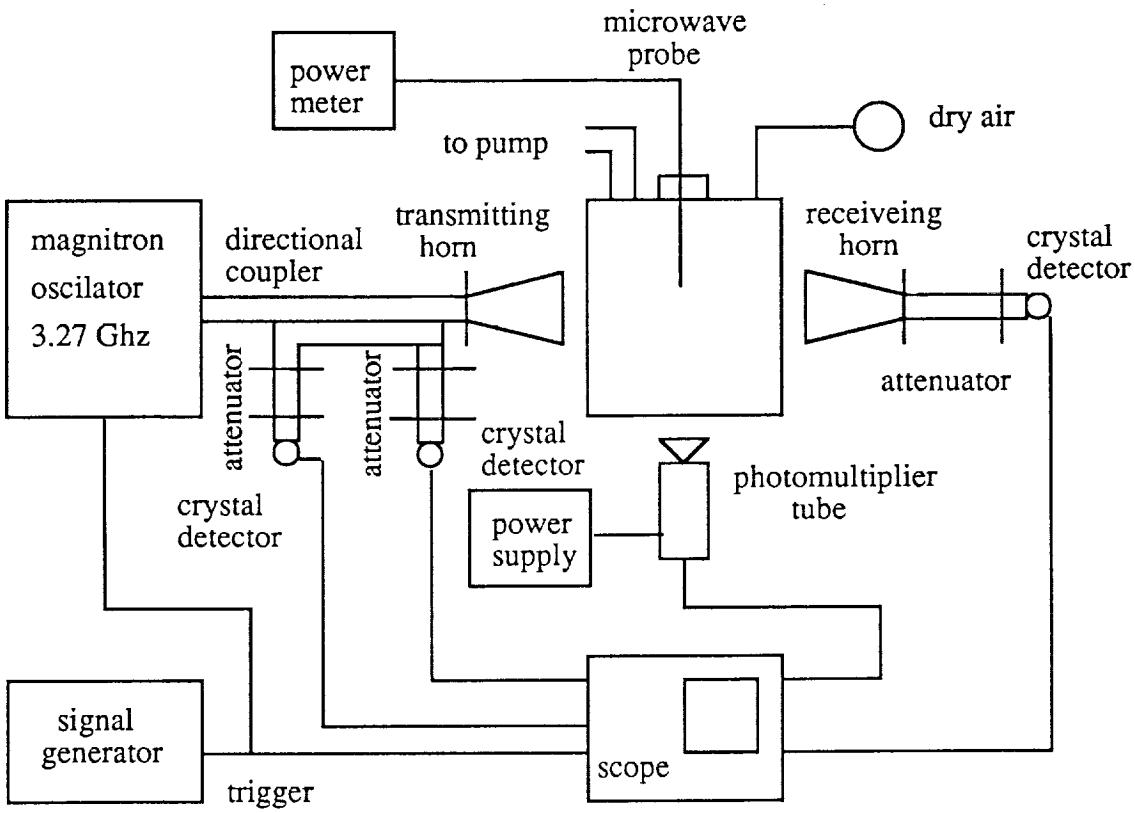

Figure 1. Experimental setup

ORIGINAL PAGE
BLACK AND WHITE PHOTOGRAPH

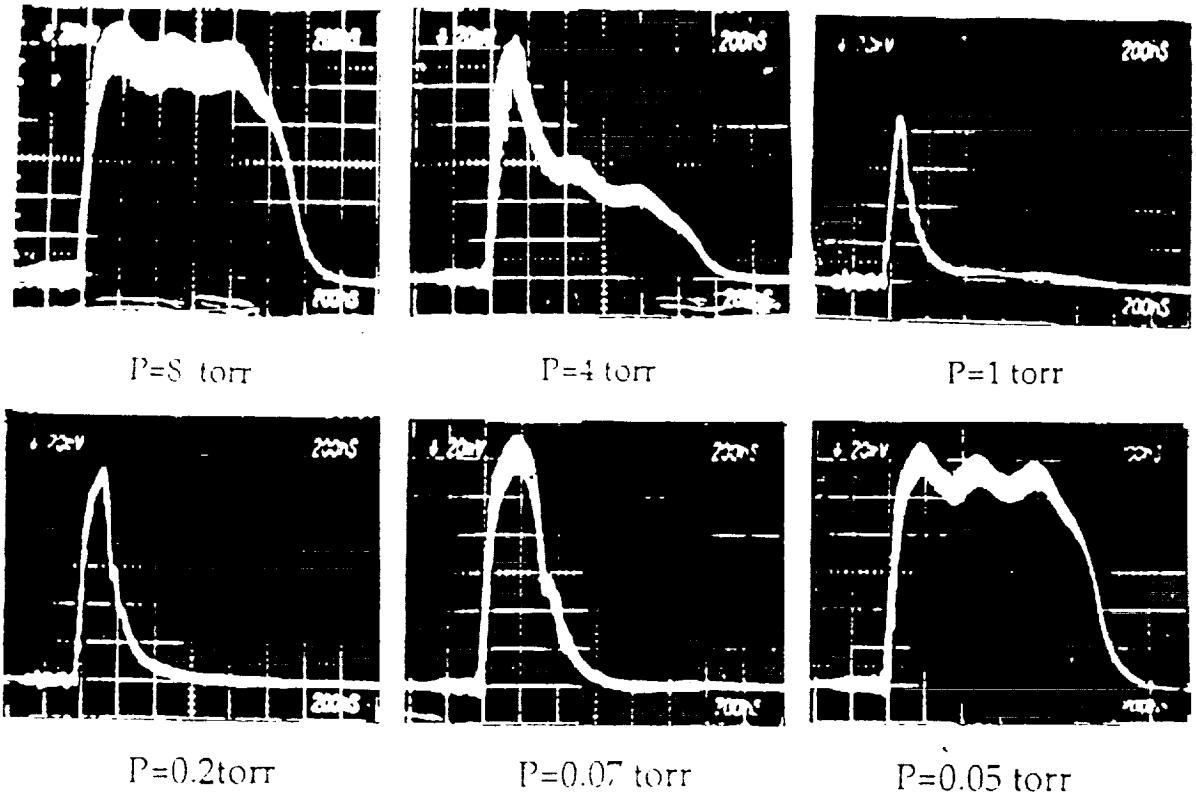

Fig. 2 Pulse transmission througth chamber at different air pressure

ORIGINAL PAGE
BLACK AND WHITE PHOTOGRAPH

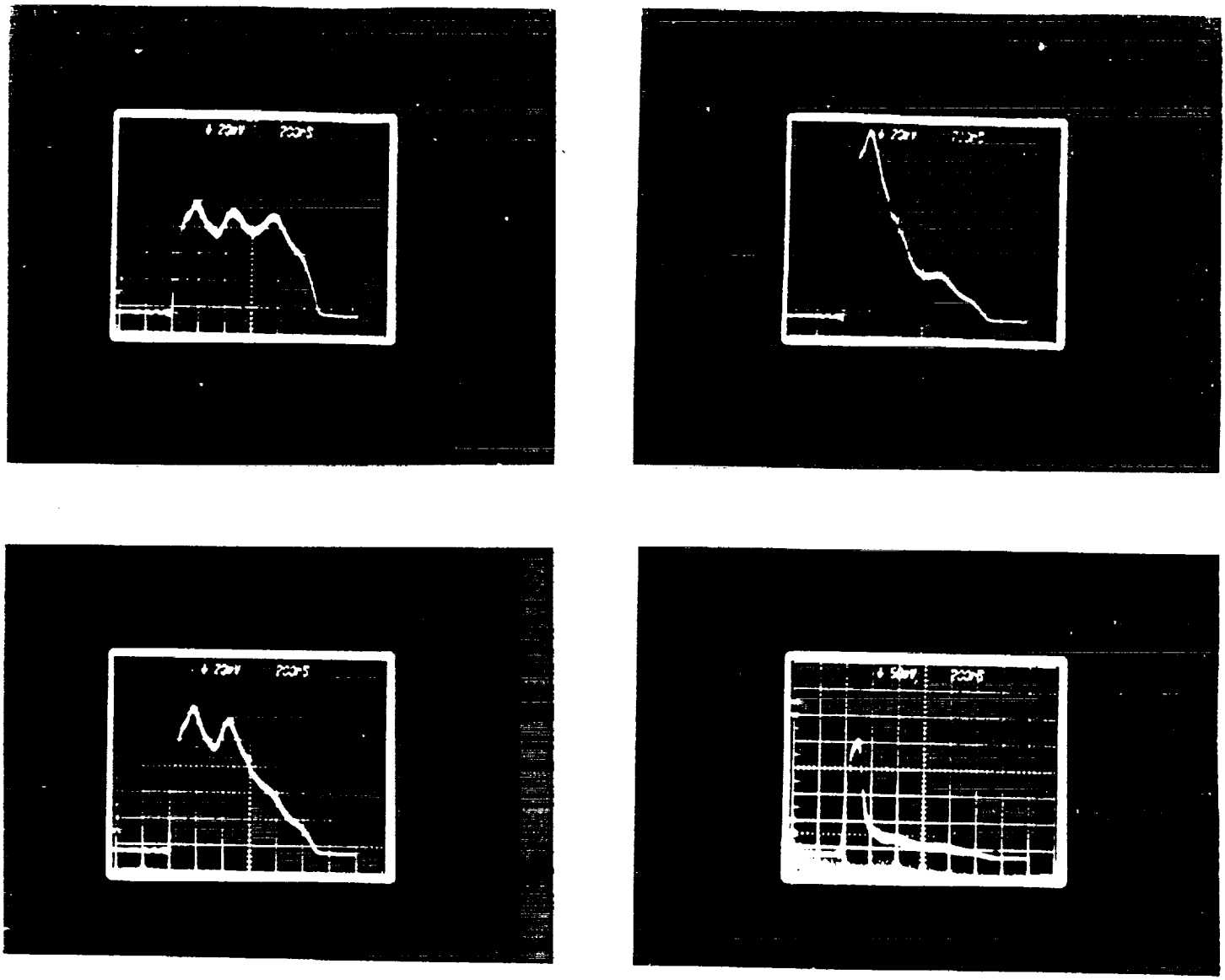

Fig.3 Tail erosion of microwave pulse

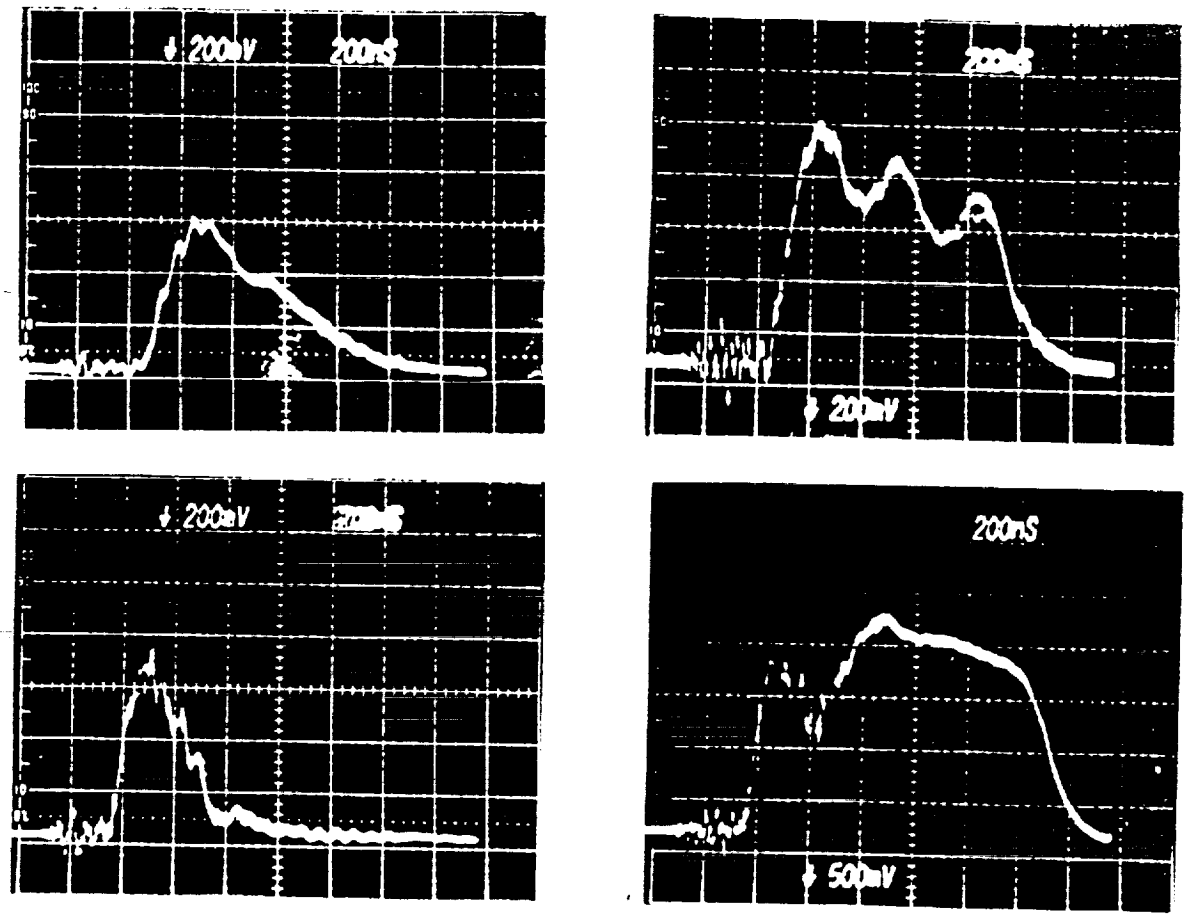

Fig.4 Transmitted pulses and the corresponding reflected pulses

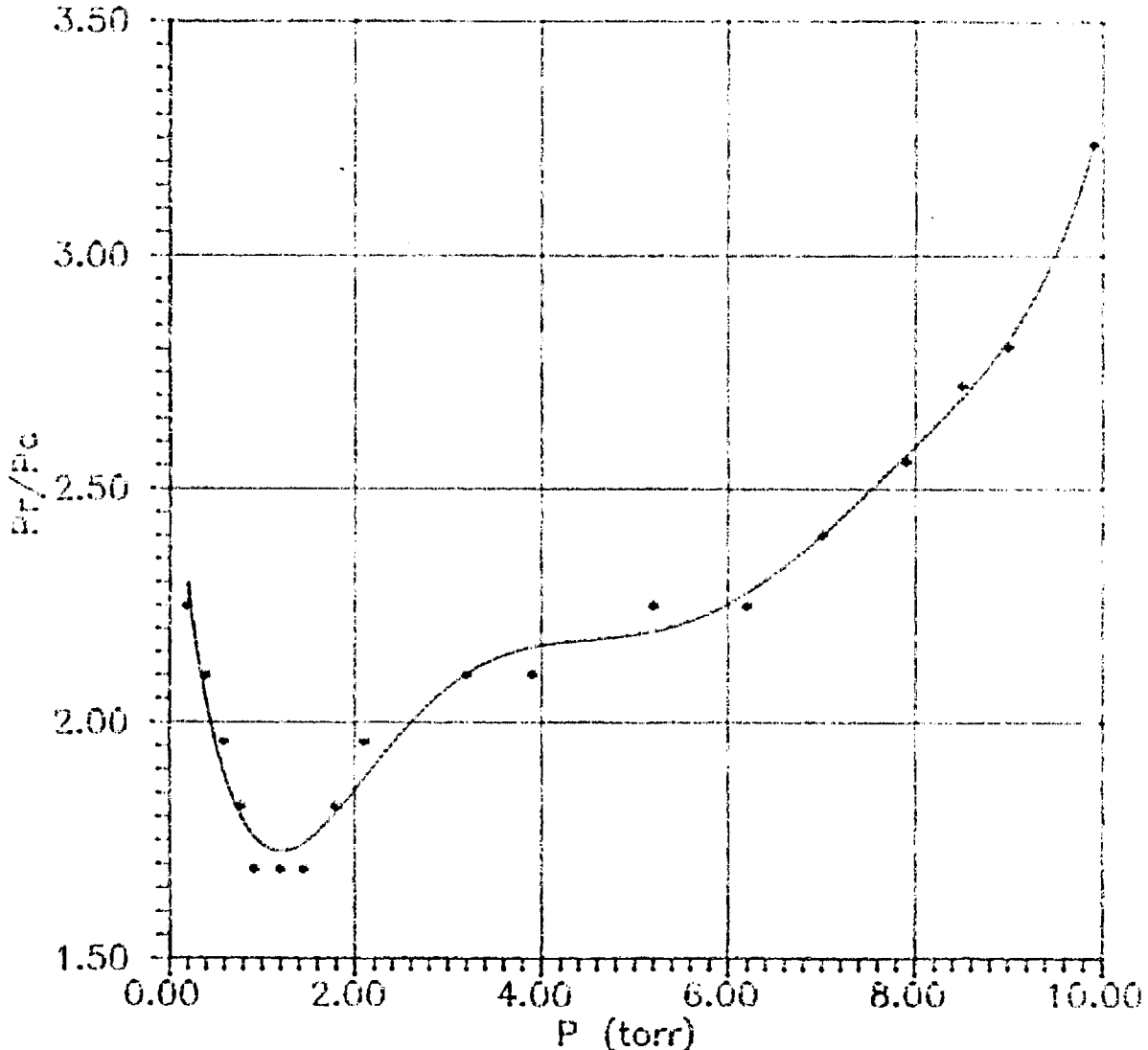

Figure 5 The dependence of the normalized critical power P=Pr/Pc on pressure for two different pulse lengths

6(a)

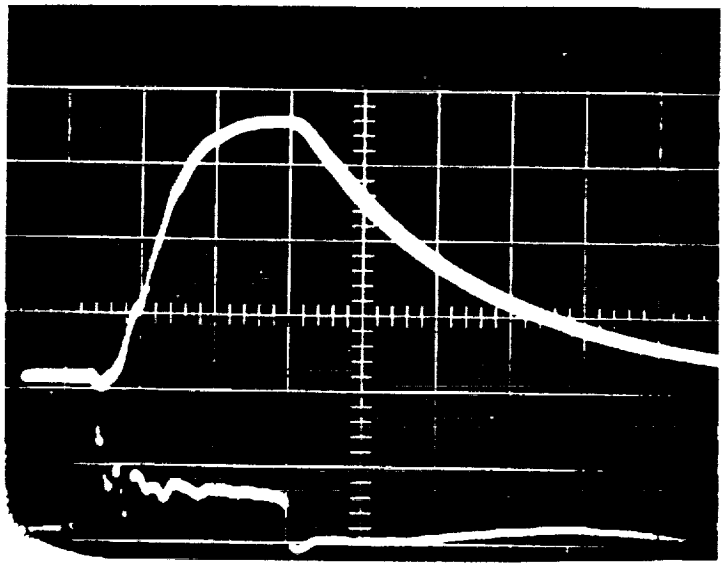

t (1μs/division)

6(b)

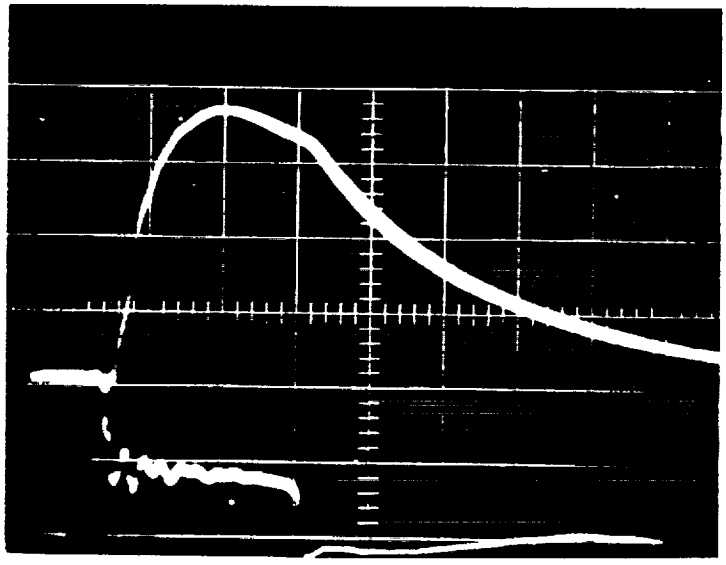

t (1μs/division)

Fig. 6 The growth and decay of enhanced airglow (upper trace). 3.3μs pulses at two different power levels P_1(for 6a) and P_2(for 6b) are used for causing air breakdown, where $P_2/P_1=1.32$. The lower trace of each photo represents the time dependance of the amplitude of microwave pulse.